Anisotropic conductivity and charge ordering in $(TMTTF)_2X$ salts probed by ESR

Claude Coulon,[1] Grégory Lalet,[1] Jean Paul Pouget,[2] Pascale Foury-Leylekian,[2] Alec Moradpour,[2] and Jean Marc Fabre[3]
[1]*Université Bordeaux 1, Centre de Recherche Paul Pascal, CNRS, UPR CNRS 8641, 115 Avenue Dr. A. Schweitzer, 33600 Pessac, France*
[2]*Laboratoire de Physique des Solides, Université Paris Sud, CNRS, UMR 8502, 91405 Orsay, France*
[3]*Architectures Moléculaires Matériaux Nanostructurés, Institut Charles Gerhardt Montpellier, UMR 5253 CNRS-UMI2-ENSCM-UM1, 8 Rue de l'école normale, 34296 Montpellier Cedex 5, France*
(Received 4 May 2007; revised manuscript received 11 July 2007; published 27 August 2007)

Single crystal ESR data on $(TMTTF)_2X$ salts are presented. Taking advantage of the large dimensions of the crystals, skin effect is studied through the asymmetry of the ESR resonance lines. When the microwave magnetic field is perpendicular to the stacking axis, a very rich temperature dependence of this asymmetry is found although the three components of the conductivity tensor often exhibit a semiconducting behavior. In particular, we show that anomalies are present when the TMTTF chains experience a Mott localization or a charge ordering. The whole set of data is discussed theoretically in relation with the anisotropy of the electrical conductivity. We show that the crystal orientation and crystal shape are crucial parameters in explaining the experimental results. More precisely, we found that at the charge ordering transition, the largest conductivity anomaly occurs along the transverse *b* direction, and we provide evidence, through ESR measurements of the conductivity in this direction, of a charge ordering transition at about 50 K in $(TMTTF)_2Br$. With the same method, we also show that irradiation kills the charge ordering transition, while deuteration enhances its critical temperature.

DOI: 10.1103/PhysRevB.76.085126 PACS number(s): 76.30.−v, 71.30.+h, 72.80.Le

I. INTRODUCTION

The family of quasi-one-dimensional molecular conductors $(TMTTF)_2X$ and $(TMTSF)_2X$ is well known to present a very rich sequence of competing ground states whose main features can be described by a unified phase diagram including sulfur and selenium salts.[1] Following this theoretical description, the competition between spin-Peierls (SP), antiferromagnetic (AF), and superconducting ground states is essentially driven by the strength of the one-dimensional (1D) Mott localization, which is known to be present for most of the TMTTF salts at ambient pressure to disappear under pressure.[2] At ambient pressure, the TMTSF salts are already metallic, while $(TMTTF)_2Br$ is at the borderline between the localized and metallic regimes. This elegant unified description seems, however, to be too simple to account for all the electronic properties among the series. Recently, charge ordered states have been reported in several TMTTF salts with octahedral anions.[3–5] Revealed more than 20 years ago by electrical conductivity and thermopower measurements,[6,7] these initially called "structureless phase transitions" have never been observed from x-ray measurements. However, the centrosymmetry of the high temperature phase must be broken at the phase transition, and the induced charge order seems to strongly influence the competition between the SP and AF at lower temperature independent of the strength of the Mott localization.[2,6,8] This new emergent problem has still to be clarified. This is important for a deeper understanding of this series of materials which are, in many respects, model systems to discuss the cumulative role of low dimensionality and electronic correlations.

In this paper, we present ESR results on several TMTTF salts. Taking advantage of the large size of the single crystals, we analyze the influence of the skin effect on the line shape. We show that this gives a very convenient contactless method in studying the electronic instabilities including the 1D Mott localization and the charge ordering. We also discuss the effect of irradiation and deuteration of the crystals with octahedral anions to emphasize the correlation existing between the charge ordering and low temperature SP instability. We also shed light on a possible charge ordering in $(TMTTF)_2Br$. The paper is organized as follows. Experimental details are presented in Sec. II. Section III is devoted to the theoretical analysis of the ESR line shape in anisotropic crystals. Description and analysis of the experimental results are developed in Sec. IV. Concluding remarks are finally given in Sec. V.

II. EXPERIMENT

A. Synthesis of the crystals

The synthesis of 98% deuterated TMTTF-d_{12} was performed according to a new procedure described elsewhere.[9] The single crystals of $(TMTTF)_2X$ or $(TMTTF\text{-}d_{12})_2X$, with $X=PF_6$, AsF_6, and SbF_6, have been grown from THF using the standard constant-current (low current density) electrochemical procedure. Single crystals of $(TMTTF)_2Br$ used in this work were synthesized for previous studies.[10,11]

B. ESR experiments

ESR experiments were made with a Bruker X band spectrometer (operating at a microwave frequency of 9.3 GHz) equipped with an ESR900 Oxford cryostat. To realize the experiment, a selected single crystal is oriented on a quartz rod and the shape of the ESR line studied for different orientations of the microwave magnetic field. When this field is along the **a** stacking axis (i.e., the largest dimension of the

needlelike crystals) the ESR line is essentially symmetric. On the other hand, a significant asymmetry was obtained for thick crystals when the microwave field is oriented perpendicular to the **a** axis. When rotating this field in the plane perpendicular to **a**, extrema of the asymmetry can be found which correspond, within the experimental error, to the extrema of the g factor. Considering the crystal structure and previous ESR studies,[12] these two cases correspond to simple orientations of the microwave field relative to conductivity tensor. When the maximum of the asymmetry is reached, the microwave magnetic field is oriented along the $g_{\max}$ direction. This implies that the corresponding microwave electric field is then located in a plane containing the chain axis (i.e., the direction of the largest electrical conductivity σ_a) and the direction of the largest transverse conductivity σ_b. When the minimum of the asymmetry is found, the microwave electric field probes the (σ_a, σ_c) plane.[13,14] These two orientations will be labeled as max and min in the following.

For each of the studied salts, several single crystals were measured. The main difference between them lies in the shape of the crystal section perpendicular to the stacking axis. Complex shapes are generally obtained with sometimes holes in their center. For this reason, we will not try to describe in detail the morphology of the crystals. Comparing experiments for different crystals of the same salt will, however, allow a discussion about the role of the crystal shape in relation with the theoretical discussion developed in the next section of this paper.

C. Irradiation procedure

Three crystals of $(TMTTF)_2AsF_6$ have been irradiated for 12 h, 1 day, and 2.7 ± 1.3 days, respectively.

The x-ray beam used for the irradiation was a white beam produced by a Philips generator equipped with a sealed tube and a copper anticathode. The power of the generator was 800 W (40 kV, 20 mA). The crystals have been placed at 100 mm from the center of the tube. The irradiation dose at this distance has been estimated using a medical dosimeter placed at the same distance as the irradiated samples. The dose then measured was around 1.2 Sv/h on the whole surface of the sample.

III. THEORETICAL APPROACH OF THE ESR LINE SHAPE

The influence of skin effect on the ESR line shape of isotropic metals has been discussed in the pioneering work of Dyson.[15] Quite generally, two characteristic lengths, the classical skin depth and the spin depth, have to be introduced, but the general theory is unnecessarily complicated in many cases.[16] In particular, a simple expression of the power absorbed by the sample can be used for fairly pure metals, when the spin depth is much larger than the classical skin depth.[16] Previous studies have shown the relevance of this approximation for organic conductors.[17] In this case, the ESR signal is the superposition of an absorption curve and a dispersion curve, i.e., the absorbed power $P(x)$ per unit surface reads

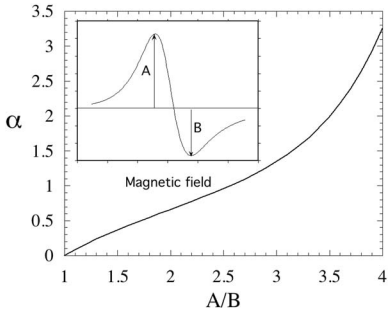

FIG. 1. Plot of α (defined in the text) versus the asymmetry A/B (defined in the inset which shows the derivative of the absorption ESR signal).

$$P(x) = \frac{1}{\sigma d}\left(\frac{\kappa(\lambda)}{1+x^2} - \frac{\nu(\lambda)x}{1+x^2}\right), \tag{1}$$

where x is the dimensionless variable which describes the distance to the resonance (field or frequency), σ is the electrical conductivity, and d is the sample thickness. This expression shows that the relevant parameter is then $\alpha = \nu/\kappa$ [the functions $\kappa(\lambda)$ and $\nu(\lambda)$ are defined in Appendix B]. For an isotropic flat plate, Eqs. (13) and (14) of Ref. 16 give the relation existing between this parameter and $\lambda = d/\delta$, where d is the plate thickness and δ is the classical skin depth [$\delta = (c^2/2\pi\sigma\omega)^{1/2}$ in cgs units, where c is the light velocity, σ is the electrical conductivity of the sample, and $\omega/2\pi$ is the microwave frequency].

Experimentally, the derivative of $P(x)$ is measured, and a symmetric signal is found when only the first term of Eq. (1) is present. When skin effect is relevant, the second term of Eq. (1) should also be considered, and an asymmetry of the ESR line ($A/B > 1$, see inset of Fig. 1) is obtained. A/B can be numerically related to the parameter α, as shown in Fig. 1.

For anisotropic samples, Eq. (1) should be generalized taking into account the different components of the conductivity tensor and the crystal shape. Let us consider the case where the microwave magnetic field is applied along one eigendirection, called **z**, of the conductivity tensor. This situation corresponds to the extremal positions discussed in Sec. II. Then, the microwave electric field lies in the $(\mathbf{x},\mathbf{y})$ plane. Penetration of this field into the crystal controls the skin effect. For this geometry, Maxwell equations depend on σ_{xx} and σ_{yy}, which are the conductivity components along the eigendirections **x** and **y**. As usual, this anisotropic problem can be mapped into an equivalent isotropic one by applying the method introduced by Van der Pauw.[18] Details of the calculation are given in Appendix A. The transformation leaves the geometry in the **z** direction unchanged but introduces a scaling in the $(\mathbf{x},\mathbf{y})$ plane such as

$$X = x\left(\frac{\sigma_{yy}}{\sigma_{xx}}\right)^{1/4} \text{ and } Y = y\left(\frac{\sigma_{xx}}{\sigma_{yy}}\right)^{1/4}, \tag{2}$$

in which the electrical conductivity of the equivalent isotropic sample is $\sigma_I = \sqrt{\sigma_{xx}\sigma_{yy}}$. At this point, the method previously introduced for isotropic solids can be used. The ab-

sorbed power is obtained by adding the contributions of the different faces of the crystal. For the considered geometry, the result will depend on σ_{xx} and σ_{yy} but also on the crystal shape, which controls the relative weight of the crystal faces. This calculation is developed in Appendix B, both in the simple case of a rectangular cross section and in the case of more complex shapes shown in Figs. 2(b) and 2(c). The parameter α can still be introduced, but it is now obtained as a sum of several contributions and therefore dependent on the conductivity tensor and on the crystal shape. The obtained expression can be expressed as a function of λ_Y (defined in Appendix B 1) and, in general, depends on three other parameters, $r=\lambda_X/\lambda_Y$, f [where $(1-f)$ measures the departure from a simple rectangular cross section], and γ which is a geometrical factor:

$$\alpha = \frac{\beta\nu(r\lambda_y) + fr^2\nu(\lambda_y) + \frac{(1-f)r^2}{(1+f)}\sqrt{1+\frac{\gamma^2}{r}}\,\nu\left(\lambda_y(1+f)\Big/\sqrt{1+\frac{\gamma^2}{r}}\right)}{\beta\kappa(r\lambda_y) + fr^2\kappa(\lambda_y) + \frac{(1-f)r^2}{(1+f)}\sqrt{1+\frac{\gamma^2}{r}}\,\kappa\left(\lambda_y(1+f)\Big/\sqrt{1+\frac{\gamma^2}{r}}\right)}.$$

Note that β, which appears in the above expression, is a simple function of f (see Appendix B 2).

Let us first consider the simplest case of a rectangular cross section. In this case, we have $f=\beta=1$, and the only remaining parameter is r. Figure 3 gives, in this case, $\alpha(\lambda_Y)$ for different values of r. For $r=1$ (isotropic case), α is a decreasing function of λ_Y, which agrees with previous studies on isotropic metals (this implies that A/B decreases as the isotropic electrical conductivity decreases). On the other hand, a more complex behavior is obtained for smaller values of r. A limiting case is obtained for $r=0$, i.e., when the conductivity along **y** is much smaller than the conductivity along **x**. In this case, a maximum of α (and therefore of A/B) is predicted when λ_Y is close to 2. This means that the line asymmetry can increase even if the two electrical conductivity components in the horizontal plane decrease. Moreover, a universal value of α close to 0.4 is expected at the maximum.

Let us now consider a more complex shape of the crystal. In the above expression, this means that one should discuss the influence of f and γ. There is, however, a simple limit obtained for $r=0$ and $\gamma \gg 1$. The latter condition implies that the contribution of the inclined faces can be neglected. As $\nu(x)$ and $\kappa(x)$ vary, respectively, as $x^4/6$ and $x^2/2$ when x goes to 0,[16] the remaining expression in this case (see Appendix B 3) is

$$\alpha_0 = \frac{f\nu(\lambda_y)}{\beta\lambda_y{}^2/2 + f\kappa(\lambda_y)}.$$

Figure 4 gives the corresponding curves $\alpha_0(\lambda_Y)$ for different values of f (in this limit, the result becomes independent of γ). A maximum of α is still observed when λ_Y is close to 2, which essentially comes from the maximum of $\nu(\lambda_Y)$, but the value of α at the maximum decreases with f.

The contribution of the inclined faces becomes important for smaller values of γ and $f \neq 1$. The extreme case where

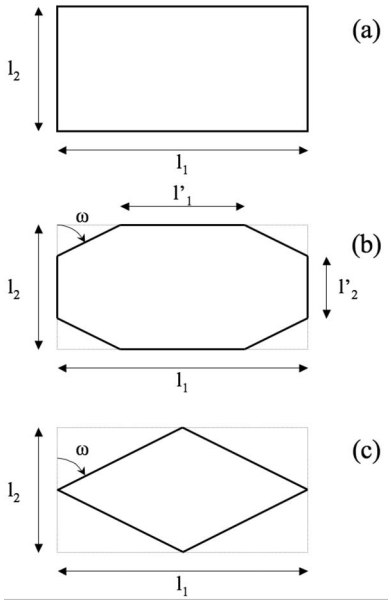

FIG. 2. View of the cross section of the crystal (perpendicular to **a**, the chain axis) as used for the calculation in Appendix B and for the discussion in Sec. III: (a) parallelepiped case, (b) a more general case, and (c) extreme situation when $f=0$ (see text).

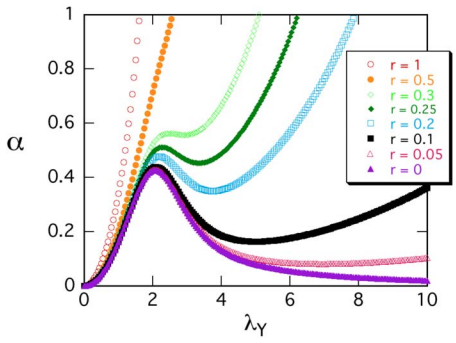

FIG. 3. (Color online) Variation with λ_Y of the parameter α for different values of r in the case of a rectangular cross section ($f=1$).

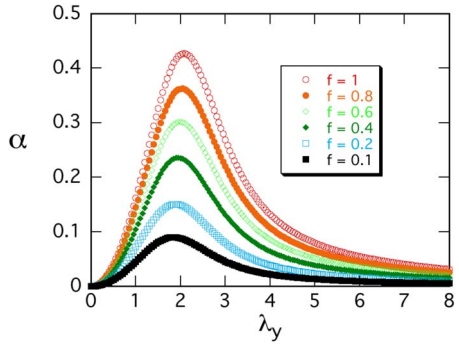

FIG. 4. (Color online) curves $\alpha(\lambda_Y)$ in the limit $r=0$ and $\gamma \gg 1$ for different values of f (these parameters are defined in Appendix B and in the main text).

$f=0$ is illustrated by Figs. 5(a) and 5(b), which correspond, respectively, to $\gamma=1$ and $\gamma=3.5$ (which are reasonable values of γ as shown in Appendix C). In these cases, a maximum of α for large λ_Y values is obtained for small r. This is consistent with the general expression of $\alpha(\lambda_Y)$ given above as the contribution of the inclined faces introduces the function $\nu(\lambda_y/\sqrt{1+\gamma^2/r})$, which goes to a maximum when $\lambda_y \approx 2\gamma/\sqrt{r}$ for small values of r. This gives for $\gamma=1$ and $r=0.05$ a maximum for $\lambda_Y \approx 9$ [Fig. 5(a)]. A similar maximum would occur for a larger $\lambda_Y \approx 30$ when $\gamma=3.5$. As for $f=1$, a plateau or even an S shape of $\alpha(\lambda_Y)$ can be observed for $f=0$. A comparison with Fig. 3 shows that the plateau may occur for larger values of λ_Y when $f \neq 1$, while the corresponding value of α strongly depends on r and γ.

To conclude this discussion, let us return to the limit where r is small. When γ is not large, the contribution of the

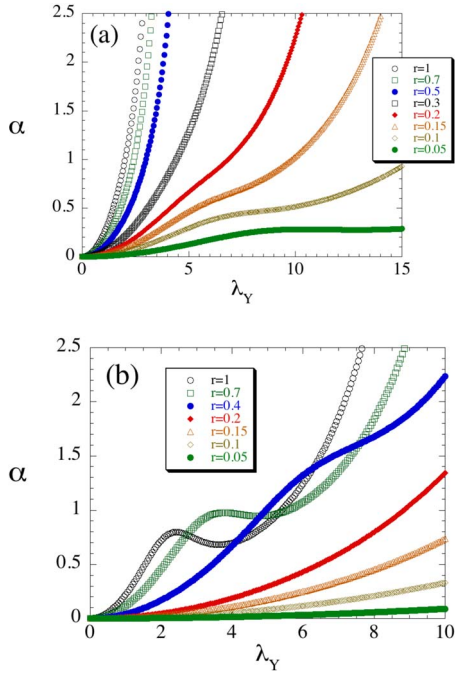

FIG. 5. (Color online) curves $\alpha(\lambda_Y)$ for $f=0$ and different values of r (these parameters are defined in Appendix C and in the main text): (a) $\gamma=1$ and (b) $\gamma=3.5$.

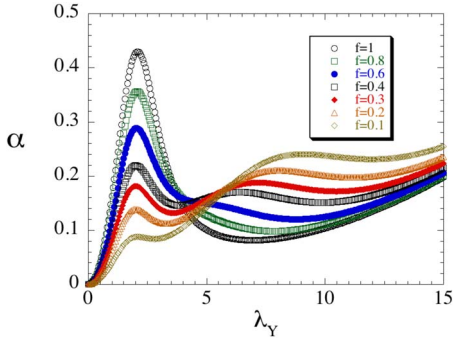

FIG. 6. (Color online) Curves $\alpha(\lambda_Y)$ for $r=0.05$ and $\gamma=1$ for different values of f.

inclined faces competes with the other terms. Figure 6 illustrates this competition for $r=0.05$ and $\gamma=1$. The obtained behavior should be compared with Fig. 4. The maximum for $\lambda_Y \approx 2$ is still observed, but a second maximum already visible in Fig. 5(a) is also present. Then, a complex figure with two maxima of comparable importance can be obtained (see, for example, the case $f=0.3$ in Fig. 6). Another consequence is that α can be almost constant over a large domain of variation of λ_Y.

The general conclusion of this study is that the departure from a rectangular section strongly affects the variations of α. To analyze the experimental results, it is important to estimate typical values of the three parameters r, f, and γ. This is the purpose of Appendix C, where we show that the $r=0$ limit can be a good approximation when the crystals are oriented in the min position while values of r between 0.5 and 1 should be considered in the max orientation. Because of the complex crystal sections, values of f and γ are less predictable and will be estimated by comparing experimental results to the theoretical predictions.

In conclusion of this part, a very rich behavior is predicted in the anisotropic case. In particular, there are situations where α and therefore A/B increase while λ_Y decreases. Moreover, the result depends on several parameters including the crystal shape.

IV. DESCRIPTION AND ANALYSIS OF THE RESULTS

This section will be organized into three successive sections to describe experimental results on $(TMTTF)_2MF_6$ salts (M=P, As, and Sb) and deuterated $(TMTTF)_2PF_6$, on $(TMTTF)_2Br$, and finally on irradiated samples of $(TMTTF)_2AsF_6$.

A. $(TMTTF)_2MF_6$ salts

Preliminary results have been presented in a previous publication mostly devoted to the study of the spin-Peierls ground state through neutron scattering experiments.[19] For the work, the 98% deuterated PF_6 salt hereafter labeled as $(TMTTF)_2PF_6$ (d_{12}) was compared to the standard (protonated) PF_6 and AsF_6 salts. In the following, these three salts will be studied in more detail through ESR data and compared with $(TMTTF)_2SbF_6$ for which a large anomaly of the

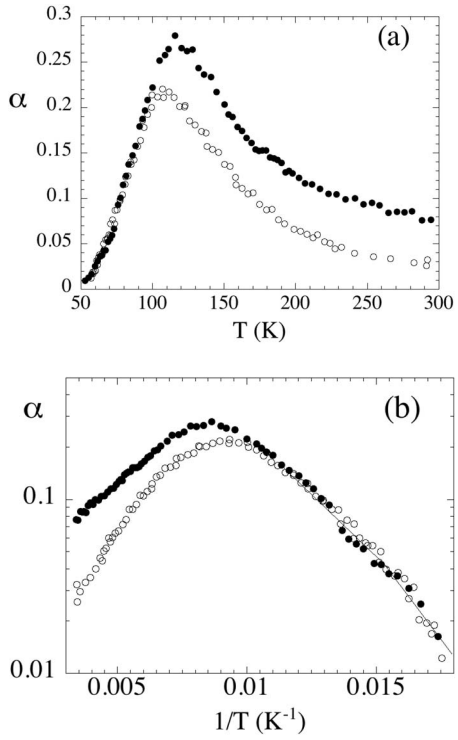

FIG. 7. (a) Temperature dependence of α obtained for two crystals of $(TMTTF)_2PF_6$ in the orientation where the minimum of asymmetry is found; (b) semilogarithmic plot showing the low temperature activated regime (note the change of slope at the charge ordering transition).

electronic properties[6,7] has been described long time ago and recently identified as a charge ordering.[8]

Figure 7 shows results obtained for $(TMTTF)_2PF_6$ in the orientation where the asymmetry is minimum. Similar results were obtained for $(TMTTF)_2PF_6$ (d_{12}) or for $(TMTTF)_2AsF_6$. Following the discussion made in the previous section, this orientation should probe the plane where the anisotropy of conductivity is maximum [i.e., the $(\mathbf{c},\mathbf{a})$ plane]. In this plane, the ratio of the components of the conductivity tensor is about 10^{-4},[13,14] and the parameter r is therefore of the order of a few 10^{-2} (see Sec. III and Appendix C). Then, the limit $r=0$ is a good approximation to describe these data at least at low temperature. In fact, the experimental curves shown in Fig. 7(a) reproduce the characteristics of the theoretical prediction shown in Fig. 4. The fact that the value of α at the maximum is sample dependent emphasizes the role of the crystal shape. Samples shown in Fig. 7 correspond to $f=0.4-0.6$ in Fig. 4. For a more quantitative comparison, it should be noted that the temperature at which α is maximum is close to 100–120 K. Comparing with the theory, this means that λ_Y should be about 2 at this temperature. From Appendix B 1, one has $\lambda_Y = b(2\pi\omega\sigma_{xx}/c^2)^{1/2}$, which is proportional to the square root of the longitudinal conductivity (along the staking axis). With $b=1$ mm and $\lambda_Y=2$, one gets $\sigma_{xx}\approx 1$ S cm^{-1}. Conductivity measurements on $(TMTTF)_2PF_6$ or AsF_6 effectively show that this value is obtained around 100 K.[2,20] Moreover, the measured room temperature conductivity being about

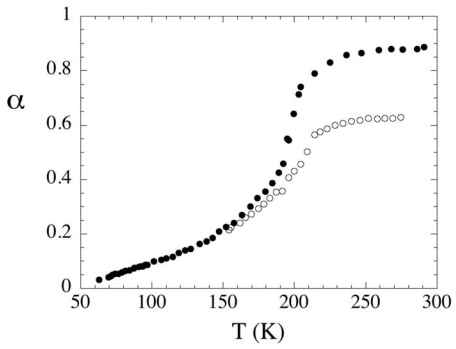

FIG. 8. Temperature dependence of α obtained for two crystals of $(TMTTF)_2PF_6$ in the orientation where the maximum of asymmetry is found.

$\sigma_{xx}\approx 20$ S cm^{-1}, we expect λ_Y to be close to 9 at 300 K. In this case, a comparison with Fig. 4 shows that the $r=0$ limit is not completely satisfactory. A small but finite value of r should be introduced to account for the room temperature value of α. On the other hand, a similar result is obtained for the two samples measured below 100 K. In this limit, we expect the development of α for small values of λ_Y to be a good approximation. As shown in Appendix B 3, α is then proportional to λ_Y^2, i.e., to σ_{xx}. A plot of $\ln\alpha$ versus $1/T$ is given in Fig. 7(b). It shows that an activated behavior is observed at low temperature with a slight change of the activation energy around $T_{CO}\approx 74$ K, the temperature of the charge ordering transition. The deduced slopes from the indicated straight lines give, respectively, 330 K (above) and 460 K (below T_{CO}). This is consistent with the previous determination of these activation energies from dc measurements.[21]

Let us now discuss the results obtained for the PF_6 or AsF_6 salts in the orientation where the maximum of asymmetry is found. Typical data are shown in Fig. 8 for $(TMTTF)_2PF_6$. Again, similar results were obtained for $(TMTTF)_2PF_6$ (d_{12}) or for $(TMTTF)_2AsF_6$. The $\alpha(T)$ dependence is first rather flat around room temperature. Then, an S shape is found around 200 K, more or less pronounced according to the shape of the crystal section. In this orientation, the $\mathbf{x}$ axis is still the chain axis, i.e., λ_Y has the same meaning as before. The main difference between the two orientations is the value of r (see Appendix C). One now probes the $(\mathbf{b},\mathbf{a})$ plane where the anisotropy of the electrical conductivity is about 10–30. For typical sample dimensions $(a/b\approx 3)$, r is therefore roughly between 0.5 and 1. As shown in Sec. III, the corresponding calculated value of α is then strongly dependent on the crystal shape. The flat part of the curves in Fig. 8 between 200 and 300 K, which is a common characteristic to all crystals, should be compared with the data shown in Fig. 5. It suggests that the $f=0$ limit is the most appropriate one to compare with the theory, with typical values of γ larger than 1 to fit with the values of α found at the plateau. Moreover, between 300 and 200 K, σ_{xx} and therefore λ_Y do not change very much with temperature, which further reinforces the possibility for a flat curve. On the other hand, when the Mott localization occurs below 200 K (i.e., below T_ρ in the literature[1]), σ_{xx} and λ_Y vary more rapidly and

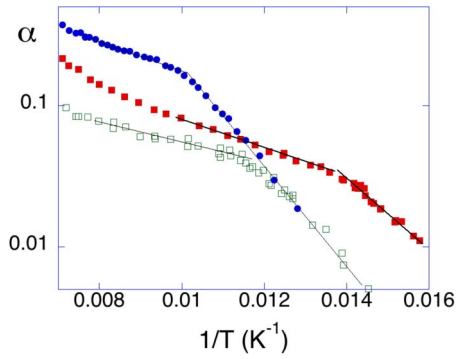

FIG. 9. (Color online) Low temperature behavior of α showing the change of slope in the semilogarithmic plot α versus $1/T$: full squares, $(TMTTF)_2PF_6$; open squares, $(TMTTF)_2PF_6$ (d_{12}); full dots, $(TMTTF)_2AsF_6$ (note the change of slope at the charge ordering transition).

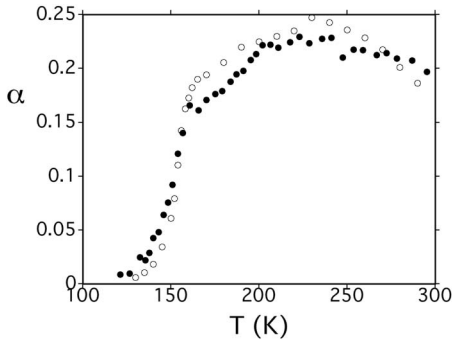

FIG. 10. Temperature dependence of α obtained for $(TMTTF)_2SbF_6$ in the orientation where the maximum of asymmetry is found (full dots). The open dots give the normalized electrical conductivity σ_b deduced from Montgomery measurements (from Ref. 22).

a quicker decrease of α can be observed whose shape is sample dependent. Further interest for this orientation is found at lower temperature. Figure 9 shows $\alpha(1/T)$ in a semilogarithmic plot for the three salts: PF_6, PF_6 (d_{12}), and AsF_6. A strong change of the slope is found in the three cases, respectively, around 72, 85, and 100 K. For example, for the PF_6 salt, the deduced activation energy is, respectively, 230 and 600 K above and below 72 K. Similar values are found for the two other compounds. For the PF_6 and AsF_6 salts, the temperature of this slope anomaly corresponds to the charge ordering critical temperature (T_{CO}) reported in the literature.[3,4] We then conclude that our ESR experiment gives an alternative and simple method to locate the charge ordering transition. In particular, we show that deuteration of $(TMTTF)_2PF_6$ induces a large increase of the charge ordering critical temperature. Moreover, it is striking that the change of the activation energy of α for this orientation is much larger than in the $(\mathbf{c},\mathbf{a})$ plane. The data are consistent with the $f=0$ limit. We show in Appendix B 3 that we essentially measure σ_b for $f=0$, when λ_Y is small and $\gamma \gg \sqrt{r}$. This means that the origin of the ESR anomaly at T_{CO} in the max orientation is essentially in the temperature dependence of σ_b. The drop of α below the charge ordering means that r decreases more rapidly and thus that σ_b increases more rapidly than σ_a. This is completely consistent with the data of Ref. 14 obtained for the AsF_6 salt, which show a larger increase of the gap of charge below T_{CO} for σ_b. Our data suggest that it is a general phenomenon for the PF_6, PF_6 (d_{12}), and AsF_6 salts. The deduced values of the activation energy above and below the charge ordering are also consistent with the results obtained by dc measurements for the AsF_6 salt.[14] In summary, our data confirm that the increase of the activation energy below T_{CO} for the longitudinal conductivity is at most of 40%, while it reaches 150% along the **b** direction.

To conclude this section, let us now describe $(TMTTF)_2SbF_6$. Samples were obtained as rather thin plates, and the majority of our measurements were made in the orientation where the asymmetry is maximum. In this case, the largest faces are horizontal and do not contribute to the signal. The remaining faces are at both ends of the crystal (perpendicular to the chain axis) or contain the chain axis. In this latter case, we essentially found inclined faces, suggesting that $f=0$ is the relevant limit to analyze the data. Figure 10 shows a typical result for this orientation. A clear anomaly is obtained at the charge ordering transition $(T_{CO}=160$ K). For a quantitative analysis of the data, one may notice that α is rather small even at high temperature. Then, when $\gamma \gg \sqrt{r}$, we essentially measure σ_b (see Appendix B 3). In fact, we show in Fig. 10 that our data can be superposed to the temperature dependence of σ_b deduced from Montgomery measurements.[22] Even the absolute value of α is correctly reproduced. With a ranging between 1.5 and 2 mm, the approximate expression given in Appendix B 3 gives $\sigma_b \approx 0.1$ S cm^{-1}, which is within a factor of 3 of the estimation deduced from standard conductivity measurements.

For one crystal, it has been possible to measure some asymmetry in the min orientation. However, nonreproducible results have been observed between 180 and 220 K probably because of the appearance of cracks or of small crystal movements. The low temperature result is reproducible and is shown in Fig. 11 where it is compared with the one obtained in the max orientation. In both directions, an activated behavior is found below the charge ordering. We find 1400

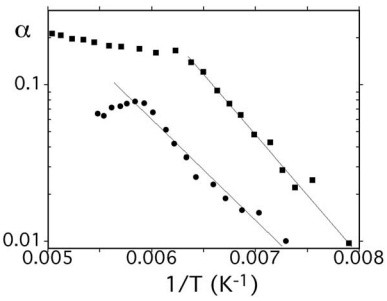

FIG. 11. Semilogarithmic plot giving α obtained for $(TMTTF)_2SbF_6$ as a function of $1/T$: full dots, in the orientation where the minimum of asymmetry is found; full squares, in the orientation where the maximum of asymmetry is found. The straight lines show the activated regimes.

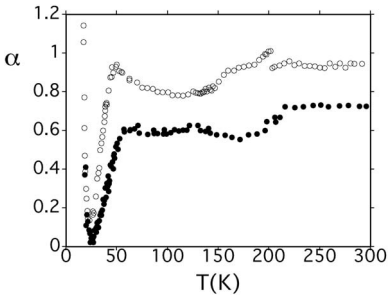

FIG. 12. Temperature dependence of α obtained for two crystals of $(TMTTF)_2Br$ in the orientation where the maximum of asymmetry is found.

and 1800 K for the min and max orientations, respectively. In the min orientation, most of the faces are vertical and $f=1$ should be a good approximation. Then, the deduced activation energy essentially corresponds to σ_a (see Appendix B 3), while we probe σ_b in the max orientation. In coherence with the other results, we therefore conclude that the maximum effect of the charge ordering concerns the **b** direction. Finally, it is interesting to remark that the min and max ESR activation energies are in fair agreement with the one deduced from the temperature dependence of σ_a and σ_b measured by the Montgomery method.[22]

B. $(TMTTF)_2Br$

Let us now discuss the results obtained with $(TMTTF)_2Br$. In this salt, a sample-dependent broad maximum of the dielectric constant has been reported at about 35–50 K,[10] and a weak slope anomaly could be detected in the thermal dependence of σ_a around 20 K.[10,11] As far as we know, up to now, no clear evidence for a charge ordering has been published for this compound.

Figures 12 and 13 give the temperature dependence of α in the max and min orientations, respectively. In the first case, two samples are compared in Fig. 12. Although the curves are slightly different, the same characteristics are found. A rather flat curve is observed down to 50 K. Then, a sharp decrease of α is found. Finally, α increases steeply below 20–25 K when approaching the antiferromagnetic ground state ($T_N \approx 13$ K).[23] In the direction where the asymmetry is minimum (Fig. 13), a smooth variation is found with a maximum around 100 K and no visible anomaly around 50 K. Again, the precursor effect for the antiferromagnetic ground state is seen as an increase of α.

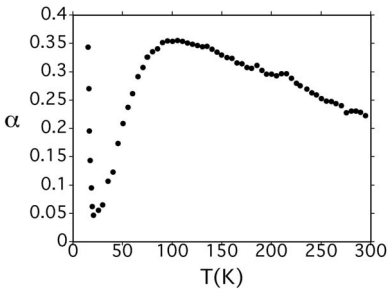

FIG. 13. Temperature dependence of α obtained for $(TMTTF)_2Br$ in the orientation where the minimum of asymmetry is found.

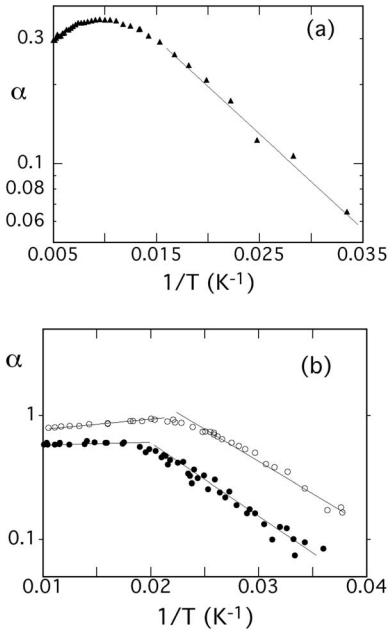

FIG. 14. Semilogarithmic plot of α as a function of $1/T$ showing the low temperature behavior for $(TMTTF)_2Br$: (a) in the orientation where the minimum of asymmetry is found and (b) in the orientation where the maximum of asymmetry is found (two different crystals).

Let us discuss these results in more detail. First, it should be noticed that for this salt, the electrical conductivity along the chain axis presents a metallic behavior down to 100 K. Moreover, the room temperature value of σ_a is about 250 S cm^{-1} to reach about 1000 S cm^{-1} at 100 K. Then, even with smaller transverse dimensions (of about 0.5 mm), we expect larger values of λ_Y (typically between 8 and 12 at room temperature). Because of the metallic behavior, this parameter should further increase down to 100 K. In this context, the maximum of α shown in Fig. 13 can be understood in the limit where r is small, noting that σ_a reaches a maximum at this temperature. It should be noted that the interpretation of this maximum is different from the one shown in Fig. 7(a) as the corresponding value of λ_Y is certainly larger than 2. In the same temperature range, only small variations of α are found in the max orientation (Fig. 12). In this case, a larger value of r (between 0.5 and 1) is expected, and Fig. 5 shows that flat parts in the $\alpha(\lambda_Y)$ curves can be obtained theoretically especially when f is close to 0. The comparison with Fig. 5 suggests that the appropriate value of γ is between 1 and 3.5. Figure 14 emphasizes the low temperature behavior. In both orientations, α becomes small at low temperature and the approximate expressions valid for small values of λ_Y become relevant. In the min orientation [Fig. 14(a)], an activated regime is found below 100 K. As for the other salts, we expect to measure in this orientation the activated behavior of σ_a. In fact, the deduced activation energy, 78 K, is in excellent agreement with the

published value obtained from longitudinal conductivity measurements.[10] The most remarkable feature is found in Fig. 14(b), which shows the data in the max orientation. As already mentioned, a clear anomaly is observed at about 50 K. A larger activation energy of about 135 K is observed below this temperature. As already shown, in this orientation, we probe the transverse conductivity σ_b. Then, our data indicate a sudden increase of σ_b. As far as we know, conductivity data along **b** are not available at this temperature for $(TMTTF)_2Br$ and this prediction remains to be confirmed. However, it is tempting to note the analogy with the data observed with the MF_6 salts (Figs. 9 and 11) to suggest the occurrence of a charge ordering transition at 50 K. The observation of a broad maximum of the dielectric permittivity around 35–50 K (Ref. 10) could be interpreted as the onset of a local ferroelectricity accompanying the charge ordering transition of $(TMTTF)_2Br$. The occurrence of a low temperature modification of the charge transport is supported by the observation below 50 K of an important increase of the thermopower in the data reported for $(TMTTF)_2Br$ (see Fig. 1 in Ref. 24 and Fig. 3 in Ref. 7). The same feature has, in fact, been already found at the charge ordering transition of the MF_6 salts.[7] Finally, it should be noticed that the observed 50 K anomaly is very sharp compared to the one observed at T_{CO} for $(TMTTF)_2PF_6$ or AsF_6. Then, one may think of a different type of charge ordering for the Br salt. However, Fig. 10 shows that a strong effect is also observed for $(TMTTF)_2SbF_6$ for which the charge ordering occurs when the electrical conductivity of the sample is still important.[25] The same argument may be applied to $(TMTTF)_2Br$ to rationalize our experimental results.

To conclude, we should note that the increase of α close to the Néel transition temperature is not surprising. Due to local fields, the ESR line is distorted close to T_N, even for small crystals. In this context, it is interesting to remark that approaching T_N from above, the critical growth of AF fluctuations probed by the EPR linewidth occurs on the same temperature range where the SP structural fluctuations vanish.[26] This effect has therefore no relation with an anomalous variation of the electrical conductivity tensor.

C. Irradiation effects in $(TMTTF)_2AsF_6$

As already mentioned, the charge ordering phase transitions found in the TMTTF series were for a long time described as structureless phase transitions as x-ray experiments always failed to bring evidence for a symmetry breaking at T_{CO}. Several experiments have been indeed attempted to evidence the symmetry breaking at T_{CO} and to directly detect the CO using x rays: (i) standard diffraction measurements of the thermal variation of Bragg reflection intensity expected to present an anomaly at T_{CO},[6,27] (ii) diffraction anomalous fine structure measurements at the sulfur K edge, (iii) extended x-ray-absorption fine structure measurements at the S and As edges,[28] and (iv) accurate electronic density measurement using structure refinement below T_{CO} to evidence the loss of inversion centers.[29] All these experiments have always failed to bring any evidence of CO. One possible explanation would be the extreme sensitivity of the samples to irradiation effects. In fact, it is now well known that the long range spin-Peierls order is very quickly destroyed by x-ray irradiation.[30] The same problem may occur for the charge ordering transition.

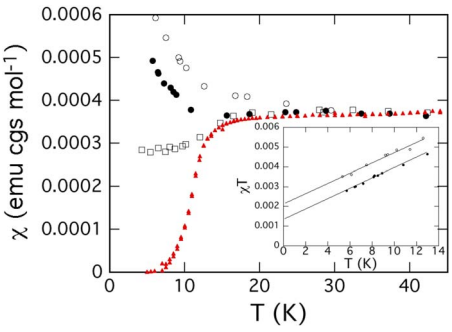

FIG. 15. (Color online) ESR spin susceptibility of irradiated $(TMTTF)_2AsF_6$ samples: open squares, 12 h; full dots, 1 day; open dots, 2.7±1.3 days; small triangles, SQUID result on the pristine sample. The plots of χT versus T are given in the inset.

ESR experiments are relevant to answer this question. Indeed, on the same crystal, the spin susceptibility can be measured to probe the spin-Peierls transition and the occurrence of a charge ordering can be discussed through the study of $\alpha(T)$. Among the three TMTTF salts which undergo a low temperature spin-Peierls ground state, the AsF_6 compound presents the highest value of T_{CO} for which the determination of the charge ordering characteristics through the ESR experiment is the easiest (see Fig. 9). We have therefore undertaken a study of the effect of irradiation on $(TMTTF)_2AsF_6$. Experimental details on the irradiation procedure are given in Sec. II.

Integration of the ESR line gives the spin susceptibility in arbitrary units. As the susceptibility is almost temperature independent between 30 and 40 K, we used the superconducting quantum interference device (SQUID) result obtained on a nonirradiated sample to normalize the ESR data. In fact, we expect the irradiation to have only a very small effect on the absolute value or the temperature dependence of the susceptibility in this temperature range. Figure 15 gives the obtained results. As expected, irradiation has a drastic effect on the spin-Peierls transition. After only 12 h of irradiation, the drop of the spin susceptibility is strongly altered. This drop completely disappears alter 1 day of irradiation and a small Curie component already appears. A stronger Curie component is found after 2.7±1.3 days of irradiation.

A quantitative estimation of the Curie component gives the amount of localized defects created by irradiation. The inset of Fig. 15 shows that the spin susceptibility can be reasonably fitted to $\chi_S = C/T + cste$, where C is the Curie constant. Extrapolating at $T=0$ K, we obtain $C \approx 0.00136$ and $C \approx 0.00217$ for 1 and 2.7±1.3 days of irradiation, respectively. This constant would be 0.375 for 1 mole of $S=1/2$ localized centers. As the spin susceptibility is normalized for a mole of TMTTF dimers, this means that about 0.18% or 0.29% of the TMTTF molecules bear a $S=1/2$ localized spin after 1 and 2.7±1.3 days of irradiation, respectively. We fi-

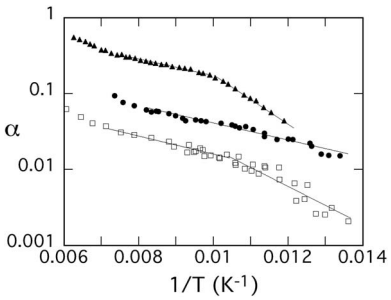

FIG. 16. Low temperature behavior of three samples of $(TMTTF)_2AsF_6$ showing the effect of irradiation on the change of slope in the semilogarithmic plot α versus $1/T$: open squares, irradiated for 12 h; full dots, irradiated for 1 day; full triangles: pristine sample.

nally estimate that about 0.1%–0.2% of $S=1/2$ localized spins per mole of TMTTF (noted below as mol % of radiation defects) are created per day of irradiation.

On the same crystals, we have studied the effect of irradiation on the charge ordering. As shown previously, the relevant experiment is the determination of α in the direction of the maximum of asymmetry. In Fig. 16, two irradiated samples (12 h and 1 day of irradiation) are compared with the pristine sample (result already given in Fig. 9). After an irradiation for 12 h, the change of slope at T_{CO} has been considerably altered (but note that T_{CO} is not substantially modified). It has almost completely disappeared after 1 day of irradiation. As expected, the sample irradiated during 2.7 ± 1.3 days (not shown) gives a similar result. Note that the absolute value of α cannot be readily compared among the samples as it depends on the crystal shape.

This result means that about 0.1–0.2 mol % of radiation defects are necessary to destroy the charge ordering transition of the TMTTF salts. Previous x-ray investigations have shown that about 0.1–0.2 mol % of radiation defects are also necessary to destroy the anion ordering transition of $(TMTSF)_2ClO_4$ (Ref. 31) and that about 0.2 mol% of radiation defects also destroyed the Peierls transition of TMTSF-DMTCNQ.[32]

The magnetic measurements reported in Fig. 15 show that about 0.1–0.2 mol % of radiation defects also destroy the SP gap in $(TMTTF)_2AsF_6$. A previous x-ray investigation of $(TMTTF)_2PF_6$ (Ref. 33) was able to show that about 0.1 mol % of radiation defects created on our x-rays experimental setup were enough to transform the SP superstructure reflections into quasi-one-dimensional broad spots. Our irradiation measurements show by comparison with those performed in Ref. 31 that the TMTTF molecule is about six times more sensitive to irradiation damages than the TMTSF molecule.

Because of the extreme sensitivity of the TMTTF molecule, 0.1–0.2 mol % of defects created on our experimental setup after an exposure time ranging from few hours (rotating anode) to one day (sealed tube)[34] are enough to destroy both the charge ordering and the SP ground states. Thus, it is virtually impossible to detect the charge ordering transition and the SP transition by x-ray diffraction. This explains why the charge ordering transition was, for a long time, described as "structureless" in the literature.

The comparable sensitivity of the spin-Peierls transition, anion ordering transition, and charge ordering transition to irradiation damages of the organic molecule is a good indication that the lattice degrees of freedom are a key parameter to stabilize the charge order in the TMTTF salts. This suggestion is evidenced by the strong dependence of T_{CO} with the nature of the anion related to its free volume in the organic cavities.[19] In addition, recent NMR experiments[35] have emphasized the role of the electron-anion coupling to stabilize the charge ordering phase.

V. CONCLUDING REMARKS

To summarize our study, we should first recall that the measure of the asymmetry of ESR lines gives a very convenient contactless method to obtain information on the conductivity tensor. In addition, ESR provides a high frequency (9 GHz) measurement of the conductivity less sensitive to the disorder because it probes local oscillations rather than large displacements of the charge carriers. This explains why the charge ordering transition is clearly visible by our measurements in the $(TMTTF)_2MF_6$ and $(TMTTF)_2Br$ salts.

This is also particularly important in probing σ_b, which is not easily obtained by standard methods. In particular, our results show that σ_b is more strongly affected at the charge ordering transition than the longitudinal conductivity σ_a. For example, we found that the gap of charge added by the charge ordering transition of $(TMTTF)_2PF_6$ is larger in the b direction ($\Delta_b^S=550$ K) than in the a direction ($\Delta_a^S=320$ K).[36] This feature is also clearly illustrated by the σ_b measurement performed in $(TMTTF)_2Br$, which exhibits a sharp drop below 50 K, while σ_a does not present a clear anomaly at this temperature. This means that any quantitative analysis of the charge ordering transition has to go beyond a 1D description. This is expected from the three-dimensional nature of the Coulomb forces existing between localized charges and if lattice displacements (such as a shift of the anions from the center of the cavities) occur at the charge ordering transition. This is also consistent with the mean field nature of this transition probed from dielectric measurements.[4]

More generally, our ESR technique gives a simple way to follow the temperature of the charge ordering when controlled modifications are imposed to a sample. In this paper, examples are given with the deuteration of the PF_6 salt or with the irradiation of the AsF_6 salt. Moreover, as ESR also gives the spin susceptibility, the correlation with the occurrence of magnetic transitions can also be studied.

Concerning this last point, our study brings appealing results in discussing the correlation between the spin-Peierls instability and the charge ordering. As already mentioned,[19] there is a clear correlation between T_{SP} (temperature of the spin-Peierls transition) and T_{CO}: $T_{SP}\approx 30\text{ K}-0.19T_{CO}$. This means that the charge ordering destabilizes the spin-Peierls ground state, in agreement with previous experimental results under pressure.[8,28] This is why the simple picture of a unified phase diagram where the competition between the spin-Peierls and antiferromagnetic instabilities would be

solely controlled by the amount of electronic localization appears too simple. In particular, our results show that with similar charge ordering transitions at 50 K, $(TMTTF)_2Br$ exhibits an antiferromagnetic ground state which contrasts with the SP one of pressurized $(TMTTF)_2AsF_6$.[37]

The above expression gives a vanishing value of T_{SP} when T_{CO} is about 160 K. In agreement with this conclusion, an antiferromagnetic low temperature ground state is found for the highly localized $(TMTTF)_2SCN$ and $(TMTTF)_2SbF_6$ salts, which present a charge ordering around 160 K.

Another important result of our study is to show that irradiation defects drastically destroy the charge and spin-Peierls long range orders. Such a finding is well documented for the Peierls transition of irradiated charge transfer salts,[32] where their understanding lies in the low dimensionality of the system. The EPR results show that irradiation creates localized spins that are tempting to associate with a localized charge. In the $(TMTTF)_2X$'s, these charges should break the long range correlation of the charge order but still preserve its short range order. In the formalism developed in Ref. 5, for a commensurate half filling, the localized charges should be located in domain walls or solitons separating charge ordered domains where the modulation exhibits a different phase with respect to the underlying lattice. The phase shift associated with a soliton should break the intrachain charge order, while the randomness of the soliton positions should break the interchain order. Inside each ferroelectric domain, a spin-Peierls instability should occur at a local scale, but the lateral disorder should prevent the establishment of a long range SP order. In addition, the presence of free $S=1/2$ spins located on the irradiation centers should strongly perturb the regularity of the SP order. In agreement with this conclusion, x-ray experiments[33] on $(TMTTF)_2PF_6$ have shown that the SP superstructure reflections disappear extremely rapidly under irradiation. Upon irradiation, the superstructure reflections are changed into diffuse lines showing that the break of interchain SP correlations is mainly responsible for the lack of long range order.

More generally, the charge order of the $(TMTTF)_2X$ seems to be very sensitive to defects. Even in nonirradiated salts, various types of structural disorders (due, for example, to the freezing at low temperature of the methyl groups or of the anion motions[35]) should limit, as discussed above, the extent of the charge order. This is particularly true for the PF_6 salt for which the dielectric constant exhibits only a broad maximum at T_{CO},[4] as usually observed in disordered ferroelectrics or "relaxors." Consistent with the above discussion, linking the charge ordering (CO) and SP orders, it is not surprising to observe, by neutron scattering[30] in the PF_6 salt, unusually weak SP superlattice reflections due to the difficulty in achieving a long range transverse order. Enhanced disorder should be present in the charge order state of $(TMTTF)_2Br$, occurring at lower temperature than in the PF_6 salt, and for which a very broad maximum of dielectric constant is observed.[10]

In conclusion, ESR seems a very promising technique in probing the electronic instabilities through the study of the line shape. In the future, we plan to deepen this discussion with the study of deuteration and irradiation of samples such as the Br, SCN, or SbF_6 salts which present a low temperature antiferromagnetic ground state.[38]

ACKNOWLEDGMENTS

We thank P. Batail, C. Lenoir, and P. Auban-Senzier for providing us samples of $(TMTTF)_2Br$, V. Cardoso for the help in the deuteration of the TMTTF molecule, and M. Imperor for the irradiation measurements. S. Ravy and S.E. Brown are also thanked for many discussions. This work was supported by the University Bordeaux I and the Conseil Régional d'Aquitaine.

APPENDIX A: ANISOTROPIC-ISOTROPIC TRANSFORMATION

We start with the Maxwell equations, making no difference between **B** and **H** (nonmagnetic medium):

$$\nabla \times \mathbf{H} = \frac{4\pi}{c}\boldsymbol{\sigma}\mathbf{E} \quad \text{and} \quad \nabla \times \mathbf{E} = \frac{i\omega}{c}\mathbf{H},$$

where $\boldsymbol{\sigma}$ is a second rank tensor with eigendirections **x**, **y**, and **z**. Assuming that **H** is along **z** (**E** in the (**x**,**y**) plane), this gives

$$\frac{\partial^2 H}{\sigma_{yy}\partial x^2} + \frac{\partial^2 H}{\sigma_{xx}\partial y^2} = -\frac{4\pi i\omega}{c^2}H.$$

The anisotropic-isotropic transformation is obtained with

$$\sigma_I = \sqrt{\sigma_{xx}\sigma_{yy}}$$

and

$$Y = y(\sigma_{xx}/\sigma_{yy})^{1/4}, \quad X = x(\sigma_{yy}/\sigma_{xx})^{1/4}, \quad Z = z.$$

This gives

$$\frac{\partial^2 H}{\partial X^2} + \frac{\partial^2 H}{\partial Y^2} = -\frac{4\pi i\omega\sigma_I}{c^2}H = -\frac{(1+i)^2}{\delta_I^2}H,$$

with $\delta_I = (c^2/2\pi\sigma_I\omega)^{1/2}$.

APPENDIX B: CALCULATION OF α FOR DIFFERENT CRYSTAL SHAPES

1. Rectangular cross section

Consider a crystal with parallelepiped shape, with a cross section shown in Fig. 2(a). The microwave magnetic field is applied along **z**. In the (**x**,**y**) plane, the dimensions of the crystal are a and l_1, respectively. The crystal dimension along **z** is called l_2. The anisotropic-isotropic transformation gives a new parallelepiped shape with dimensions

$$\theta_y = l_1(\sigma_{xx}/\sigma_{yy})^{1/4} \quad \text{and} \quad \theta_x = a(\sigma_{yy}/\sigma_{xx})^{1/4},$$

with the third dimension l_2 being unchanged.

The absorbed power is readily obtained from Eq. 12 of Pifer and Magno (Ref. 16) after weighting the term of a given face by its surface:

$$P(x) \propto \frac{l_2\theta_Y}{\sigma_I\theta_X}\left|\frac{\kappa(\lambda_X)}{1+x^2}-\frac{\nu(\lambda_X)x}{1+x^2}\right|+\frac{l_2\theta_X}{\sigma_I\theta_Y}\left|\frac{\kappa(\lambda_Y)}{1+x^2}-\frac{\nu(\lambda_Y)x}{1+x^2}\right|,$$

with

$$\lambda_X=\frac{\theta_X}{\delta_I}=\frac{a(\sigma_{yy})^{1/2}}{(c^2/2\pi\omega)^{1/2}} \quad \text{and} \quad \lambda_Y=\frac{\theta_Y}{\delta_I}=\frac{l_1(\sigma_{xx})^{1/2}}{(c^2/2\pi\omega)^{1/2}}=\lambda_X/r,$$

where

$$\delta_I=\frac{c}{(2\pi\sigma_I\omega)^{1/2}}.$$

In this expression, the functions $\kappa(\lambda)$ and $\nu(\lambda)$ are defined by

$$\kappa(\lambda)=\frac{2\sin\lambda\sinh\lambda}{(\cosh\lambda+\cos\lambda)^2},$$

$$\nu(\lambda)=\frac{\sinh^2\lambda-\sin^2\lambda}{(\cosh\lambda+\cos\lambda)^2}.$$

Note that we choose a definition of $\nu(\lambda)$ which is the opposite of the one given in Ref. 16 [Eq. 14] in order to introduce a positive parameter.

$P(x)$ can be expressed under the form

$$P(x)\propto\frac{l_2}{\sigma_I}\left(\frac{1}{1+x^2}\right)\left[\frac{\theta_Y}{\theta_X}\kappa(\lambda_X)+\frac{\theta_X}{\theta_Y}\kappa(\lambda_Y)\right]-\frac{l_2}{\sigma_I}\left(\frac{x}{1+x^2}\right)\left[\frac{\theta_Y}{\theta_X}\nu(\lambda_X)+\frac{\theta_X}{\theta_Y}\nu(\lambda_Y)\right].$$

This gives a generalization of Eq. (1) of Sec. III, and the expression of for reads

$$\alpha=\frac{\nu(\lambda_X)+\left(\frac{\theta_X}{\theta_Y}\right)^2\nu(\lambda_Y)}{\kappa(\lambda_X)+\left(\frac{\theta_X}{\theta_Y}\right)^2\kappa(\lambda_Y)},$$

with

$$r=\frac{\lambda_X}{\lambda_Y}=\frac{a}{l_1}\left(\frac{\sigma_{YY}}{\sigma_{XX}}\right)^{1/2}.$$

The above expression finally reads

$$\alpha=\frac{\nu(r\lambda_Y)+r^2\nu(\lambda_Y)}{\kappa(r\lambda_Y)+r^2\kappa(\lambda_Y)}.$$

2. More complex shape

In practice, the section of the crystals in the plane perpendicular to the stacking axis is rather complex and sample dependent. To present a simple discussion on the effect of the crystal shape, we consider the crystal section shown in Fig. 2(b). Through this example, we like to discuss the role of the faces which are neither perpendicular nor parallel to the microwave field. This situation is commonly observed with $(TMTTF)_2X$ salts which present a triclinic unit cell. Although complex crystal sections are observed experimentally, we choose here an ideal situation which allows us to extrapolate between a rectangular [Fig. 2(a)] and a lozenge-like section [Fig. 2(c)]. More precisely, we take

$$\frac{l_1'}{l_1}=\frac{l_2'}{l_2}=f.$$

Then, $1-f$ measures the relative amount of inclined faces. The limit $f=0$ is shown in Fig. 2(c). The above equation means that we have chosen $l_1/l_2=\tan\omega$ [see Fig. 2(b)]. The calculation is the same as before. First, an anisotropic-isotropic transformation is applied. Then, the contribution of the different faces is calculated to sum these contributions. There are now three terms: for each vertical face,

$$P(x)\propto\frac{l_2f\theta_X}{\sigma_I\theta_Y}\left|\frac{\kappa(\lambda_Y)}{1+x^2}-\frac{\nu(\lambda_Y)x}{1+x^2}\right|$$

for each cross section,

$$P(x)\propto\frac{\beta l_2\theta_Y}{\sigma_I\theta_X}\left|\frac{\kappa(\lambda_X)}{1+x^2}-\frac{\nu(\lambda_X)x}{1+x^2}\right|,$$

where $\beta=1-(1-f)^2/2$ comes from the estimation of the surface of the cross section, and for each inclined face,

$$P(x)\propto\frac{l_2(1-f)\theta_X}{2\sigma_I(1+f)\theta_Y\cos\omega'}\left|\frac{\kappa(\lambda_d)}{1+x^2}-\frac{\nu(\lambda_d)x}{1+x^2}\right|,$$

where ω' is the transformed value of ω, i.e., $\tan\omega'=\theta_Y/l_2$ and $\lambda_d=\lambda_Y(1+f)\cos\omega'$. In the prefactor of this expression, one has the surface of the face and also a $\cos\omega'$ factor to account for the projection of the microwave field in the horizontal plane. Moreover, we have

$$\frac{1}{\cos\omega'}=\sqrt{1+\tan^2\omega'}=\sqrt{1+\frac{a}{l_1r}\tan^2\omega},$$

where r has the same definition as above. This expression can be still simplified by introducing a purely geometrical factor $\gamma=\sqrt{a/l_1}\tan\omega$:

$$\frac{1}{\cos\omega'}=\sqrt{1+\frac{\gamma^2}{r}}.$$

The final expression for α is

$$\alpha = \frac{\nu(r\lambda_y) + \frac{fr^2\nu(\lambda_y)}{\beta} + \frac{(1-f)r^2}{\beta(1+f)}\sqrt{1+\frac{\gamma^2}{r}}\,\nu\left(\lambda_y(1+f)\Big/\sqrt{1+\frac{\gamma^2}{r}}\right)}{\kappa(r\lambda_y) + \frac{fr^2\kappa(\lambda_y)}{\beta} + \frac{(1-f)r^2}{\beta(1+f)}\sqrt{1+\frac{\gamma^2}{r}}\,\kappa\left(\lambda_y(1+f)\Big/\sqrt{1+\frac{\gamma^2}{r}}\right)}.$$

For $f=1$, this expression becomes equivalent to the one obtained for a rectangular section. In the general case, there are essentially two new parameters, f and γ, as β is a function of f. Typical values of these parameters are specified in Appendix C.

3. Simple limits

In some cases, a simplification of the general expression of α is possible. Firstly, simplified expressions are available when r is small. In this situation, two cases should be distinguished:

(1) If f is not small, the contribution of the inclined faces can be neglected for moderate values of λ_Y, and a simple limit is obtained where

$$\alpha(0,f) \approx \frac{f\nu(\lambda_y)}{\frac{\beta\lambda_y^2}{2} + f\kappa(\lambda_y)}.$$

In this limit, γ plays no role and the only remaining parameter is f.

(2) If r and f are simultaneously small, the contribution of the inclined faces is relevant, and a more complete expression should be considered ($\beta \approx 1/2$ in this limit):

$$\alpha(0,f) \approx \frac{f\nu(\lambda_y) + \frac{\gamma}{\sqrt{r}}\nu\left(\frac{\sqrt{r}\lambda_y}{\gamma}\right)}{\frac{\lambda_y^2}{4} + f\kappa(\lambda_y)}.$$

The crossover induced by the competition between the two terms of the numerator is discussed in Sec. III (see Fig. 6).

Secondly, if λ_Y is small, all the functions appearing in the expression for α can be developed at their lowest order. This gives

$$\alpha = \frac{\beta r^2 + f + (1-f)(1+f)^3\left(1+\frac{\gamma^2}{r}\right)^{-3/2}}{\beta + f + (1-f^2)\left(1+\frac{\gamma^2}{r}\right)^{-1/2}}\frac{\lambda_y^2}{3}.$$

In particular, when $f=1$ (rectangular shape), this implies (c is the light velocity)

$$\alpha = (r^2+1)\frac{\lambda_y^2}{6} = \frac{\pi\omega}{3c^2}(a^2\sigma_{yy} + l_1^2\sigma_{xx}).$$

A mixture of the conductivities σ_{xx} and σ_{yy} is measured. When $f=0$ (lozenge), one has

$$\alpha = \frac{r^2 + 2\left(1+\frac{\gamma^2}{r}\right)^{-3/2}}{1 + 2\left(1+\frac{\gamma^2}{r}\right)^{-1/2}}\frac{\lambda_y^2}{3}.$$

In particular, if $\gamma^3\sqrt{r} \gg 1$ and $\gamma \gg \sqrt{r}$, the approximate expression

$$\alpha \approx r^2\frac{\lambda_y^2}{3} = \frac{\lambda_x^2}{3} = \frac{2\pi\omega}{3c^2}a^2\sigma_{yy}$$

shows that σ_{yy} is essentially measured.

APPENDIX C: RELEVANT PARAMETERS IN THE min AND max ORIENTATIONS

Let us discuss the meaning and typical values of the relevant parameters in the two studied orientations.

1. min orientation

In this case, the microwave magnetic field is oriented along the $\mathbf{b}'$ axis and the microwave electric field probes the $(\mathbf{a},\mathbf{c}^*)$ plane. Then, $l_1=b$, $l_2=c$, and λ_Y is proportional to $b(\sigma_a)^{1/2}$ and $r=(a/c)(\sigma_c/\sigma_a)^{1/2}$. Introducing a typical value for the conductivity anisotropy, this gives $r \approx 0.016a/c$ at room temperature. For the PF_6 or AsF_6 salts discussed in Sec. IV, where $a/c \approx 3$, this gives $r \approx 0.05$ and the $r=0$ limit is a first approximation. However, finite values of r should be considered for thin samples. For example, for $(TMTTF)_2SbF_6$, the ratio a/c is typically ten times larger and $r \approx 0.5$. An intermediate situation is found for the Br samples for which typical values of r are around 0.1.

The other relevant parameters are f and γ. Considering that the relative orientation of the faces is usually determined by the crystal structure, expected values for the angle ω (defined in Fig. 2) can be anticipated. In the min orientation, $\mathbf{b}^*$ is approximately vertical and $\mathbf{c}^*$ is approximately horizontal. Then, $\omega=60°$ is expected if the perpendicular to the inclined face is $\mathbf{b}^*+\mathbf{c}^*$. For $a/c \approx 3$, typical values of γ are, in this case, about 3.5. However, various and complex crystal sections are found and smaller values of ω are expected. If $\omega=30°$ and $a/c \approx 3$, γ is about 0.9. Then, we will consider γ as an adjustable parameter with typical values between 1 and 4. In the same way, we will explore any possibility with $0<f<1$.

2. max orientation

In this case, the microwave magnetic field is oriented along the $\mathbf{c}^*$ axis and the microwave electric field probes the $(\mathbf{a},\mathbf{b}^*)$ plane. Then, $l_1=c$, $l_2=b$, and λ_Y is proportional to $c(\sigma_a)^{1/2}$ and $r=(a/b)(\sigma_b/\sigma_a)^{1/2}$. Introducing a typical value for the conductivity anisotropy, this gives $r\approx 0.23a/b$ at room temperature. When $a/b\approx 3$, this gives $r\approx 0.7$. This is a typical value for most of the samples in this orientation. As previously explained, we will consider f and γ as adjustable parameters with $0<f<1$ and $1<\gamma<4$.

[1] C. Bourbonnais and D. Jérome, Science **281**, 1155 (1988).

[2] For a recent review, see C. Coulon, J. Phys. IV **114**, 15 (2004).

[3] D. S. Chow, F. Zamborszky, B. Alavi, D. J. Tantillo, A. Baur, C. A. Merlic, and S. E. Brown, Phys. Rev. Lett. **85**, 1698 (2000).

[4] P. Monceau, F. Ya. Nad, and S. Brazovskii, Phys. Rev. Lett. **86**, 4080 (2001).

[5] For a recent review, see S. Brazovskii, in *Organic Conductors*, edited by A. Lebed, Springer Series in Physics (Springer, New York, in press); arXiv:cond-mat/0606009.

[6] R. Laversanne, C. Coulon, B. Gallois, J. P. Pouget, and R. Moret, J. Phys. (Paris), Lett. **45**, L393 (1984).

[7] C. Coulon, S. S. P. Parkin, and R. Laversanne, Phys. Rev. B **31**, 3583 (1985).

[8] W. Yu, F. Zamborsky, B. Alavi, A. Baur, C. A. Merlic, and S. E. Brown, J. Phys. IV **114**, 35 (2004).

[9] A. Moradpour (unpublished).

[10] F. Nad, P. Monceau, and J. M. Fabre, Eur. Phys. J. B **3**, 301 (1998).

[11] S. Tomic, N. Biskup, S. Dolanski Babic, and K. Maki, Europhys. Lett. **26**, 295 (1994).

[12] C. Coulon, P. Delhaès, S. Flandrois, R. Lagnier, E. Bonjour, and J. M. Fabre, J. Phys. (Paris) **43**, 1059 (1982).

[13] Anisotropy of the electrical conductivity is described in P. Auban-Senzier, D. Jérome, C. Carcel, and J. M. Fabre, J. Phys. IV **114**, 41 (2004); J. Moser, M. Gabay, P. Auban-Senzier, D. Jérome, K. Bechgaard, and J. M. Fabre, Eur. Phys. J. B **1**, 39 (1998).

[14] B. Korin-Hamzic, E. Tafra, M. Basletic, A. Hamzic, and M. Dressel, Phys. Rev. B **73**, 115102 (2006).

[15] F. J. Dyson, Phys. Rev. **98**, 349 (1955).

[16] J. H. Pifer and R. Magno, Phys. Rev. B **3**, 663 (1971).

[17] S. Baudron, P. Batail, C. Coulon, R. Clérac, E. Canadell, V. Laukhin, R. Melzi, P. Wzietek, D. Jérome, P. Auban-Senzier, and S. Ravy, J. Am. Chem. Soc. **127**, 11785 (2005).

[18] L. J. Van der Pauw, Philips Res. Rep. **16**, 187 (1961).

[19] J. P. Pouget, P. Foury-Leylekian, D. Le Bolloc'h, B. Hennion, S. Ravy, C. Coulon, V. Cardoso, and A. Moradpour, J. Low Temp. Phys. **142**, 147 (2006).

[20] A similar conclusion is deduced from the data of Ref. 14 after correcting the crack contribution.

[21] F. Ya. Nad, P. Monceau, C. Carcel, and J. M. Fabre, Phys. Rev. B **62**, 1753 (2000).

[22] In the Montgomery method, the electrical contacts are placed at the four corners of the crystal. It gives the two components of electrical conductivity tensor in the corresponding plane, H. C. Montgomery, J. Appl. Phys. **42**, 2971 (1971). We have used this technique to deduce the transverse conductivity in $(TMTTF)_2SbF_6$, R. Laversanne and C. Coulon (unpublished).

[23] S. S. P. Parkin, J. C. Scott, J. B. Torrance, and E. M. Engler, Phys. Rev. B **26**, 6319 (1982).

[24] K. Mortensen, E. M. Conwell, and J. M. Fabre, Phys. Rev. B **28**, 5856 (1983).

[25] The sharpest change of Δ is observed at the CO transition if, using the notations of Ref. 36, Δ^b is weak above T_{CO}, i.e., if the salts are well conducting above T_{CO} or equivalently if T_ρ is close to T_{CO}.

[26] J. P. Pouget and S. Ravy, Synth. Met. **85**, 1523 (1997).

[27] P. Foury-Leylekian, S. Ravy, and J.-P. Pouget, Physica B **312-313**, 574 (2002).

[28] S. Ravy, P. Foury-Leylekian, D. Le Bolloc'h, J.-P. Pouget, J. M. Fabre, R. J. Prado, and P. Lagarde, J. Phys. IV **114**, 81 (2004).

[29] P. Fertey (unpublished).

[30] P. Foury-Leylekian, D. Le Bolloc'h, B. Hennion, S. Ravy, A. Moradpour, and J.-P. Pouget, Phys. Rev. B **70**, 180405(R) (2004).

[31] R. Moret, J. P. Pouget, R. Comès, and K. Bechgaard, J. Phys. (France) **46**, 1521 (1985).

[32] L. Forro, L. Zuppiroli, J. P. Pouget, and K. Bechgaard, Phys. Rev. B **27**, 7600 (1983).

[33] J. P. Pouget (unpublished).

[34] Measurement of the irradiation dose shows that our monochromatized experimental setup operating with a 1500 W sealed tube generator (used to study the SP transition) creates the same amount of defects (0.1–0.2 mol % per day) as a white beam produced with an 800 W sealed tube generator used for the irradiation performed in the present study. With the 12 kW rotating anode generator used to collect the data of Ref. 27, the irradiation dose is nine times larger.

[35] W. Yu, F. Zhang, F. Zamborszky, B. Alavi, A. Baur, C. A. Merlic, and S. E. Brown, Phys. Rev. B **70**, 121101(R) (2004).

[36] In the TMTTF salts, the gap of charge (Δ) is the quadratic sum of the gap of charge due to the charge localized on the bonds (Δ^b), which develops below T_ρ, and the one due to the charge localized on the sites (Δ^S), which develops below T_{CO}: $\Delta^2=(\Delta^b)^2+(\Delta^S)^2$ (Ref. 5).

[37] F. Zamborszky, W. Yu, W. Raas, S. E. Brown, B. Alavi, C. A. Merlic, and A. Baur, Phys. Rev. B **66**, 081103(R) (2002).

[38] In particular, preliminary results show that irradiation has the same effect on σ_b at the CO transition of $(TMTTF)_2SbF_6$ and Br as the one observed here on the AsF_6 salt, C. Coulon and J. Boulon (unpublished).